SOME CURRENT RESEARCHES INTO FUNDAMENTAL ASPECTS OF INGOT STRUCTURE

J.Beech and G.J.Davies

Department of Metallurgy
University of Sheffield, Sheffield, U.K.

1. Introduction

Although the development of surface and internal structures in solidifying ingots has been the subject of study for many years, there are still a number of unresolved problems. In recent years as the demand for high quality ingots has increased there has been increased emphasis on fundamental studies. In many instances existing information has formed a basis for the subsequent elucidation of a problem. This paper describes results from three related studies in which structure development has been investigated with a view to improving product quality.

The studies deal with (a) the practical aspects of ingot skin formation and a theoretical analysis and appreciation of the problems involved, (b) a consideration of blow-hole structures and the development of a new technique for assessing the "gas potential" of a steel melt and (c) the direct observation of the first stages of channel formation using a specially constructed cell to simulate ingot behaviour.

2. The Development of Surface Structures

Irregularities such as ripples and laps on the surface of as-cast products have long been recognised and a comprehensive study by Waters[1] was the beginning of efforts to define the nature of metallic surfaces under various conditions of solidification.

Waters and Thornton[2] proposed a model for ripple and lap formation based on solidification over the meniscus as the metal rose in the mould (fig.1). In figure 1(a) the solid extends to the point 'a' and does not grow over the meniscus. Later, the solid has grown over the meniscus (figure 1(b)) and this situation prevents the liquid metal from

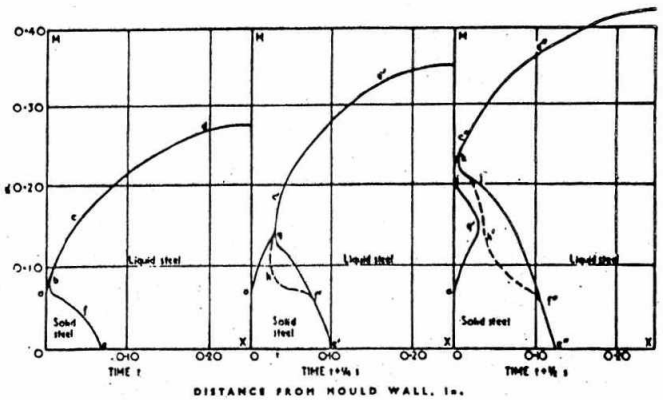

Fig.1 Ripple formation mechanism in ingots as proposed by Thornton.

contacting the mould. Eventually the ferrostatic pressure causes the solid meniscus to deform and then the metal recontacts the mould wall. It has also been proposed in similar circumstances that shrinkage effects[3] are responsible for the inward movement of the shell rather than the shell being associated with the shape of the meniscus.

The object of the present work was, therefore, to establish unambiguously the effect of experimental variables on ripple formation, to carry out critical experiments to elucidate the mechanism and to develop heat flow model for the initial stage of solidification.

2.1 Experimental Procedure

Experimental ingots were produced using an uphill teeming technique. The design used (fig.2) a CO_2-sand running system dimensioned to minimise turbulence. Different sizes of choke, located at the bottom of the sprue, were used to vary the rate of entry of metal into the mould and hence the rate of rise. The mould consisted of four plates, 75mm wide, 25mm thick and 300mm high made from either mild steel or water-cooled copper which were either assembled inside the

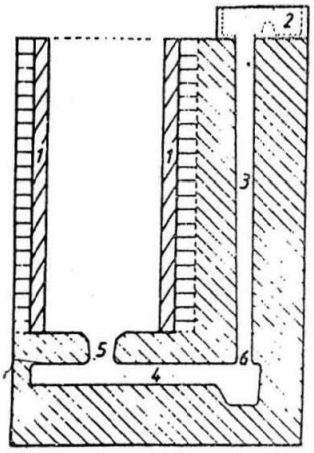

Fig.2 CO_2-sodium silicated system used in the laboratory scale ingot casting experiments.

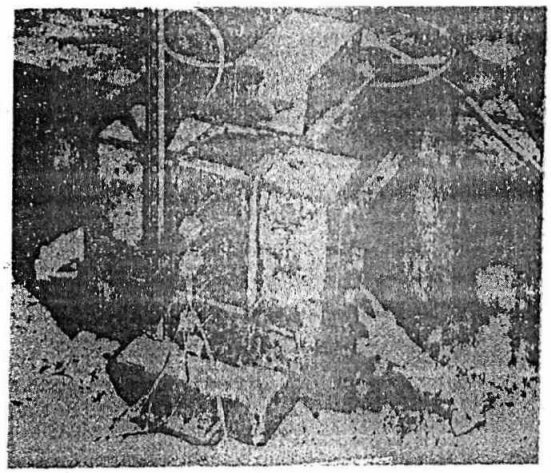

Fig.3 The mould assembly

sand mould or just clamped together. The faces of the plates in contact with the melt were machined to the different roughness levels and as appropriate coated with carbon black. A water-cooled copper mould assembly is shown in figure 3.

Steels with carbon contents in the range 0.003 to 1.63wt.% were induction melted, the superheat adjusted and the ingots teemed.

2.2 Results

(a) Surface finish of the mould

Figure 4 shows the faces of a 0.2wt.% steel ingot cast using mild steel plates as mould walls. Each of the four plates has a different surface condition. Face (a) was grooved vertically at a pitch of 1mm and depth of 0.4mm. Faces (b) and (c)

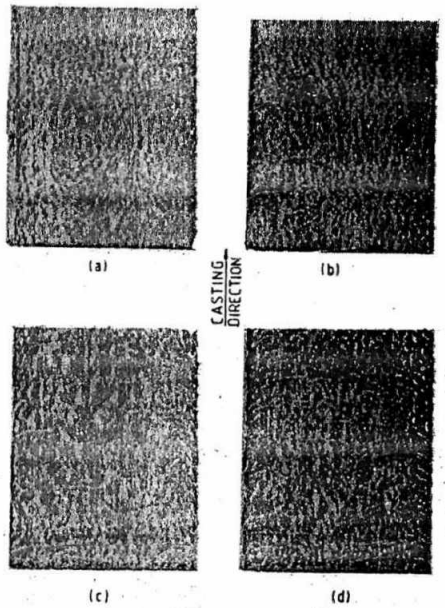

Fig.4 Surfaces of a 0.2%C steel ingot showing the effect of mould roughness on the degree of rippling. Roughness decreases (a)-(d). Pencil rubbing.

were prepared with horizontal and vertical lines respectively, and in each case the lines were 0.6mm apart and 0.1mm deep. Face (d) had a ground finish.

The melt in contact with face (a) reproduces the lines scribed on the mould with peak to valley depths 0.2mm less than those of the mould. No ripples were produced on this surface.

The lines on faces (b) and (c)were not reproduced and ripples were formed, which were more severe in the corners. The most severe rippling was found on face (d) and this was found to be similar even with finer surface finishes in other experiments. The increased heat flux associated with a water cooled copper mould is evidenced by the greater width and depth of ripples in the latter case compared with a mild steel mould having the same surface finish. When carbon black was used on a plate surface the degree of rippling was reduced.

(b) Chemical composition

For the same casting conditions the severity of surface rippling decreased as the carbon content increased. For carbon contents up to about 0.2wt.% the most severe rippling was observed with a noticeable decrease as the carbon content increased above this value.

At 1.5wt.%C surface rippling was only produced with superheats of less than 15°C, casting speeds below 3mm min^{-1}, a strong chill and a smooth mould, For example, with mild steel plates a ground surface finish was necessary. In 0.2wt.%C alloys a high superheat of about 100°C and a rough surface finish were required to eliminate ripples.

(c) Superheat and casting speed

As the melt rose in the ingot both speed and metal temperature were reduced and the severity of rippling, as measured by the number of ripples in a given ingot length, increased.

As the melt superheat was increased, the rippling was eliminated and about 0.6wt.%C a value of about 60°C was adequate for this purpose.

At rates of rise less than 2mm min^{-1} rippling is most likely to occur.

2.3 Microstructure in the Vicinity of Ripple/Lap

The dendritic growth is strongly oriented in the region that is flat and has obviously solidified in contact with the mould wall. In figure 5, the lap, which has a curvature similar to the meniscus, has various oriented dendrites associated with it. Above the lap when the metal has resumed contact with the mould the strongly oriented dendrites return. The fan-shaped dendrites in figure 6(a) show

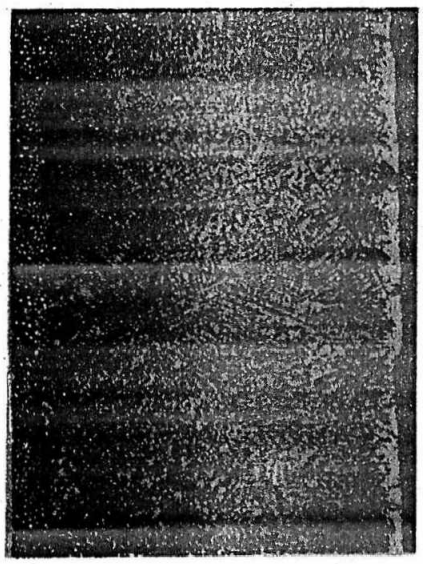

Fig.5 Structure in the ripple region of a 0.1%C steel.

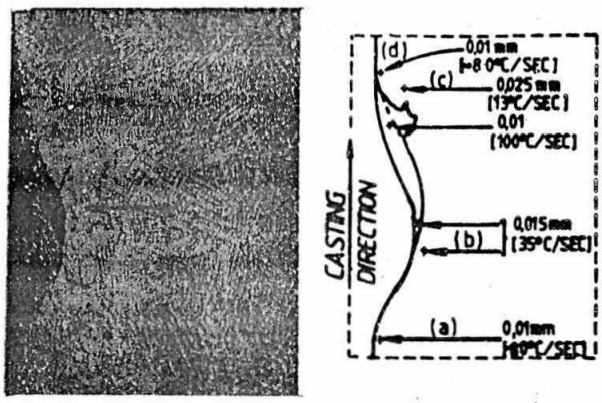

Fig.6 (a) Bending of an originally lapped interface.

(b) Values of dendrite arm spacings and cooling rates in the vicinity of a surface ripple.

that the solid formed can be subsequently bent back towards the mould. In addition an indication of the rates of solidification can be obtained from measurements of the dendrite arm spacings figure 6(b). Those parts solidified in contact with the mould are seen to have cooling rates about twice those associated with the lapped region.

2.4 A Bismuth Ingot

Since it has been suggested that shrinkage plays an important role in ripple formation, an ingot of bismuth was cast since it expands on freezing. The same features were observed as those found in steels, showing that the presence of a shrinkage force is not an essential prerequisite for ripple formation.

3. A Theoretical Model of Skin Formation

The observations are consistent with a mechanism that requires that, during periods of time when there is good thermal contact at or near the meniscus, the solid shell grows partially over the meniscus. It should, therefore, be possible to characterise and determine the severity of surface features such as ripples from the first principle of heat transfer and solidification.

3.1 The Basic Model

A plane is considered which is transverse to and incorporates the meniscus and is located at the midface of the ingot

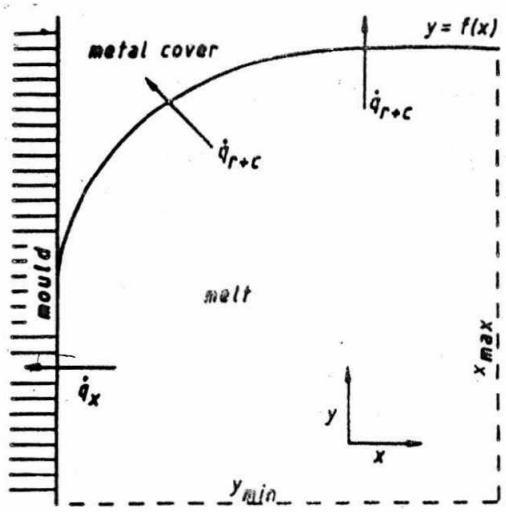

Fig.7 The physical system used as a basis for heat transfer analysis at the meniscus. q_r = radiant heat flux, q_c = conduction heat flux.

(figure 7) at the moment when contact with the mould occurs. It is envisaged that the meniscus formed against the mould wall be maintained static, or nearly so, for a short time. The aim is to investigate whether in this time solid can be formed over the meniscus. The model does not consider either the effects of turbulence, remelting or deformation of the solidifying shell.

3.2 Meniscus Shape

The shape of the meniscus was obtained from the as-cast shape of laps which agreed closely with that obtained from direct observations made using a mould with quartz window. An empirical equation was fitted to the curve:-

$$Y = U\,(1 + \exp(-BX))^z \qquad (1)$$

U relates to the meniscus height whilst B and z are constants which determine the shape of the curve.

Using equation (1) and superimposing a square grid on the physical model in figure 7 the nearest intersection points in the vertical direction were calculated. These points were then used to calculate the stair-like geometry M(i) as shown in figure 8. This new geometry contains nodes with associated volume elements of different size and subjected to different boundary conditions. The table summarises these volume elements and the characteristics used for the calculations.

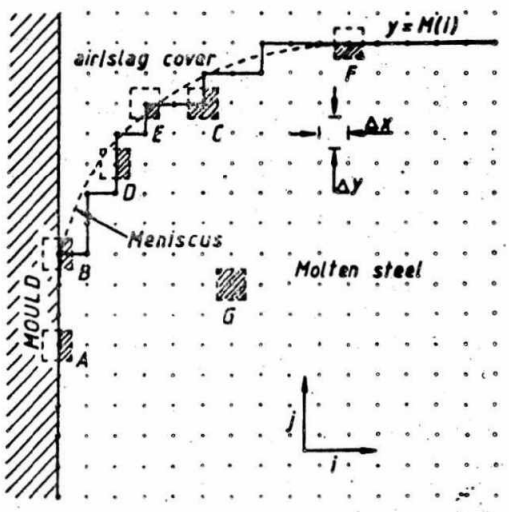

Fig.8 Idealisation of the physical system of fig.7 showing the geometry of the volume elements.

3.3 The Governing Equation

For the case of a two dimensional analysis the equation that describes heat transfer under transient flow conditions[4] is:-

$$\frac{1}{\rho}\left[\frac{\partial}{\partial x}\left(k\frac{\partial T}{\partial x}\right) + \frac{\partial}{\partial y}\left(k\frac{\partial T}{\partial y}\right)\right] = \frac{\partial H}{\partial t} \qquad \ldots\ldots\ldots\ldots\ldots\ldots (2)$$

This equation was solved for the volume elements given in the table using a numerical procedure. Explicit expressions for enthalpy were derived using a finite difference method. This method was chosen because it makes the handling of the latent heat of solidification easier.

3.4 Boundary Conditions

The starting conditions for the system in figure are:-

(i) $T_{(i,j)} = T_M \quad X = 0 \quad y \geqslant 0 \quad t \geqslant 0$

(ii) $T_{(i,j)} = T_A \quad X > 0 \quad y > M(i) \quad t \geqslant 0$

(iii) $T_{(i,j)} = T_p \quad X \quad 0 \quad y < M(i) \quad t = 0$

where T_M, T_A and T_p are the mould, air/slag cover and pouring temperatures, respectively.

Heat transfer at the interface is defined by:-

(iv) $-k\left(\frac{\partial T}{\partial x}\right) = o \quad x = x_{max} \quad y \geqslant 0 \quad t > 0$

(v) $-k\left(\frac{\partial T}{\partial y}\right) = \phi \quad x \geqslant 0 \quad y = 0 \quad t > 0$

(vi) $-k\left(\frac{\partial T}{\partial y}\right) = h_{CON}\left[T_{ij} - T_A\right] \quad x > 0$
$y = M(i) \quad t > 0$

(vii) $-k\left(\frac{\partial T}{\partial y}\right) = \sigma\varepsilon\left[T_{ij}^4 - T_A^4\right] \quad x > o \quad y = M(i) \quad t > 0$

(viii) $-k\left(\frac{\partial T}{\partial y}\right) = h\left[T_{ij} - T_m\right] \quad x = o$
$y = M(i) \quad t > 0$

Substitution of these conditions into equation (2) enable the thermal state of the system to be calculated at any time.

Having calculated the enthalpy content at any stage the physical state, liquid, solid or liquid-plus-solid, of the element is identified. This enables the fraction solid and temperature to be determined and new properties can then be assigned for the next step of the calculation.

The fraction solid at any time can be calculated from

$$f_s = \frac{H_L - H_{ij}}{H_L - H_S}$$

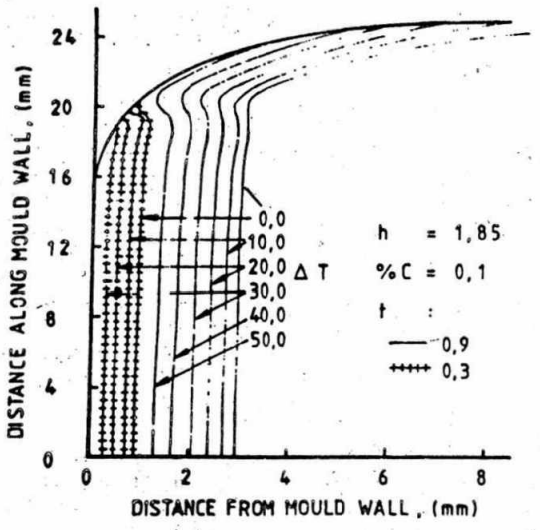

Fig.9 The influence of superheat on the formation of the surface solid skin. Results are shown for $f_s = 0.3$ and $f_s = 0.9$.

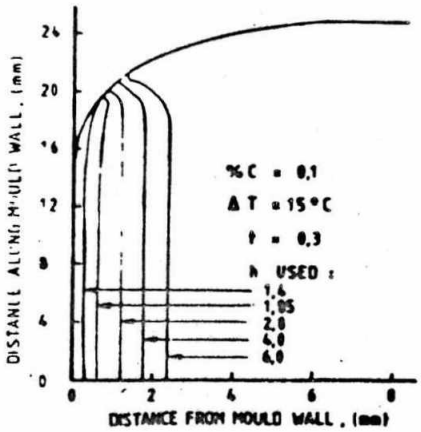

Fig.10 The effect of the interface heat transfer coefficient on skin formation.

3.5 Results

Influence of superheat

Using a metal-mould transfer coefficient (h) of 1.85 $KWm^{-2}K^{-1}$ and considering the thickness of the solid skin at 0.3 and 0.9s the influence of superheat for a 0.1wt.%C steel is seen in figure 9. The skin thickness decreases as the superheat is increased assuming negligible proportions at the higher values.

Mould-metal heat transfer coefficient(h)

Figure 10 shows the decrease in skin thickness, predicted by the model, as the values of h decrease. With very rough surfaces the values of h may be less than those used in the calculation. Agreement with experiment is good, with the rough surfaces producing less freezing over the meniscus and consequently fewer and shallower ripples.

Chemical composition

The model predicts that freezing over the meniscus will be a maximum at about 0.2wt.% carbon (figure 11) and this relates directly to the difficulties reported earlier in the experimental results in producing a ripple free surface at this carbon level.

3.6 Conclusions

The experimental results are consistent with a meniscus freezing mechanism for the production of surface ripples and laps. The curvature of the latter always relates to the meniscus outline and the

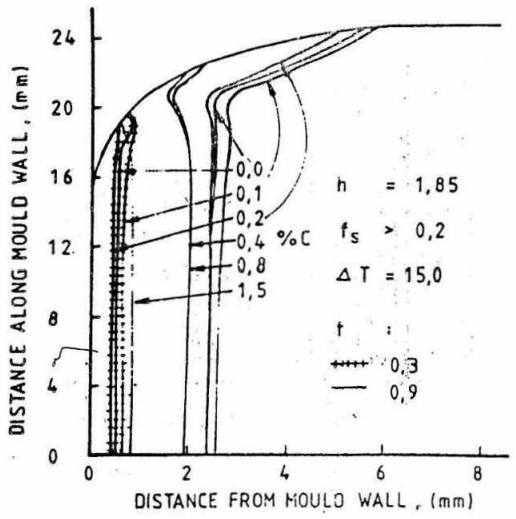

Fig.11 The effect of C content on skin formation. Results are shown for f_s = 0.3 and f_s = 0.9.

influence of experimental variables is readily explicable on the basis of meniscus freezing. The experiment using bismuth showed clearly that shrinkage was not necessary for ripple formation and so lent further support to the proposed mechanism.

The theoretical model, reported only briefly, has predicted the influence of superheat and mould condition but also explained the influence of carbon, showing maximum rippling at about 0.2wt.% carbon. The latter effect had previously been explained on a shrinkage-based model.

4. The Blow-hole Structure of Ingots

An example is shown in figure 12 of how the surface condition can influence the presence of blow-holes in its proximity. In this case gas evolution was vigorous but blow-holes were seen only in the regions where the liquid had contacted the mould surface. The work reported in the previous section showed that the surface layer of an ingot forms very quickly and that this rate is decreased somewhat in regions which solidify away from the mould walls such as, for example, the miscus region. This decrease in the rate may be sufficient to allow blow-hole "nuclei" to escape or the (unspecified) nuclei may be unable to form without mould/metal contact.

Whatever the source of blow-holes, it is necessary in most types of steels to control the gas content of the melt since this provides the driving force for

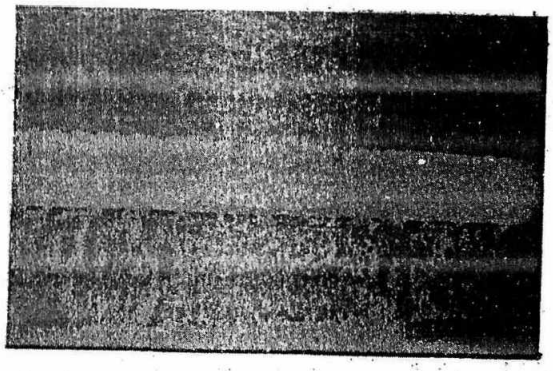

Fig.12 The influence of surface condition on the occurrence of sub-surface blowholes.

the growth of the nuclei to blow-holes. Either it is required to remove all blow-holes or, as in balanced and rimming steel, to control them. There are a number of models to predict blow-hole growth and again these rely on a knowledge of initial gas contents.

Oxygen probes have been used to good effect and it has proved possible to base production methods for balanced steels on the results obtained from them. However, this is never done with complete certainty and some of the difficulties are usually associated with the uncertainty of the hydrogen and nitrogen contents present. It was envisaged that a "total gas content" may be measured prior to teeming if a first bubble technique such as that used in aluminium could be developed. The aim of the work was, therefore, to assess the validity of such an approach.

4.1 A Justification of the First Bubble Technique

The technique used for many years in the aluminium industry merely consists of pouring a sample into a crucible which is held at constant temperature and then evacuating the chamber that holds the crucible. When the first bubble appears on the surface the pressure is observed. The elemental gas content is then determined either directly from Sievert's Law or from a suitable calibration. The technique at first sight is a crude one but some theoretical justification has been offered[5] for its success.

It has been established that liquids can trap air in cavities in the walls of containers. Figure 13 shows one possible situation and it can be seen that the air pocket (or embryo bubble) can increase in volume initially as the radius of curvature r increases

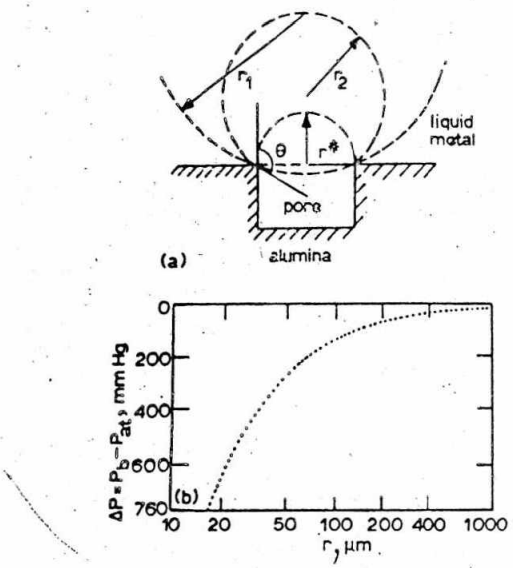

Fig.13 (a) A schematic representation of bubble growth from a cavity.

(b) The pressure required for bubble growth versus radius of the cavity.

up to abour r_1. As shown r_1 is negative but the sign depends on the contact angle, θ, and r_1 could be positive in the case where $\theta < 90^o$. The volume of the embryo bubble may increase due to a reduction in external pressure, an ingress of gas or a rise in temperature. However, at the mouth of the cavity r_1 has decreased and is now equal to r*.

For the embryo to mature into a bubble which will be released spontaneously and eventually be of radius r_2, for example, r must first decrease from r_1 to r* and the radius of curvature of the gas-liquid interface should not become less than the critical r* as the bubble grows, i.e. $r > r^*$ and the volume of the embryo V must be greater than V*, the critical volume.

If we now assume that the cavity which is to provide the nucleation site is at a depth h below the surface of the metal, the pressure above the melt is P_{at} the radius of curvature of the embryo r, the gas/liquid surface energy γ, and the pressure inside the bubble P_b then:

$$P_b - (P_{at} + P_h) = \frac{2\gamma}{r} \qquad (3)$$

A reduction in pressure above the melt P_{at} in the absence of gas will not allow r to decrease since P_b will also decrease as the volume of the embryo bubble increases. Similarly an increase in temperature of the gas inside the embryo will also increase the volume of the embryo but will not in itself provide the driving force of a reduction in r.

However, when gas is present P_b will be in equilibrium with the gas concentration in the metal and according to Sievert's Law:

$$= K\sqrt{P_g} \qquad (4)$$

As the volume of the embryo increases more gas will diffuse into it and P_b will be maintained. Hence when P_{at} has been reduced sufficiently to satisfy equation (3) with $r = r^*$, the embryo bubble can mature and a bubble will be released.

Putting $r = r^*$ and rearranging equation (1) gives,

$$P_b - P_{at} = \frac{2\gamma}{r^*} + P_h \qquad (5)$$

The difference between P_b and P_{at}, ΔP, depends critically on r*, Assuming h = 50mm and $\gamma = 10^{-5}$g mm^{-2} a curve of P versus r was drawn fig.13(b). In view of the uncertainty of the γ value the exact position of the curve is not known but it is sufficiently accurate for some general conclusions to be drawn. The ΔP value is small (<100 mmHg) down to $r \sim 100\mu$m but with an r value of 10μm the nucleation site would not be effective.

The observations recorded here show gas bubbles can be released at various pressures depending upon the gas content of the melt. There is no difficulty in nucleation and therefore ΔP cannot be large. Pores in the crucible of radius about 40μm could act as nucleation sites at low ΔP values.

Substituting equation (5) into equation (4) and rearranging yields,

$$kx_g^2 = \frac{2\gamma}{r} + P_h + P_{at} = C + P_{at} \qquad (6)$$

if r and h are constant x_g is clearly related to P_{at}.

Obviously if r changes drastically from melt to melt C will change and the technique will become unreliable. The presence of suitable nucleation sites is therefore essential if reproducible results are to be obtained. Theoretically, therefore, a combination of gases can produce the same effect with each one contributing to the value of P_g.

5. The first Bubble Technique in Steel

In the case of steel the practical problems in using such a technique and the theoretical analysis is obviously more complex.

5.1 Experimental Arrangement

Figure 14 shows the alumina crucible, which is to receive the steel, surrounded by a graphite susceptor placed inside a larger alumina crucible. The whole assembly is situated in an induction coil operating at a frequency of 3kHz. The coil is placed inside a vacuum chamber (fig.14).

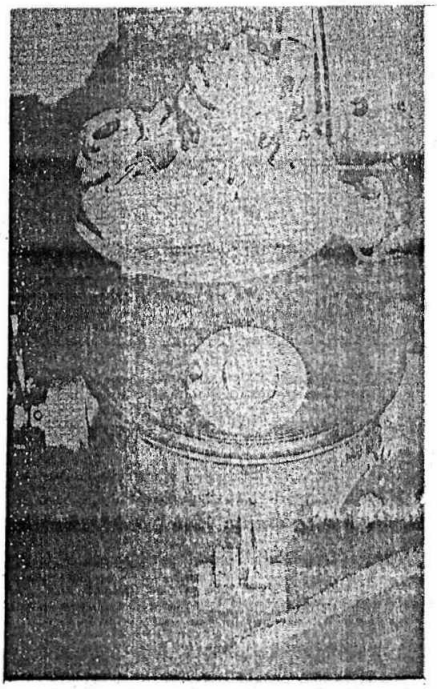

Fig.14 The experimental arrangement for the first bubble technique for steels.

Steel is transferred from a melting furnace and poured into the inner alumina crucible which is held at 1600°C. The lid is placed on the vacuum chamber and the latter is evacuated as the melt surface is observed. The pressure is noted as the first bubble appears.

In some cases an ingot was cast from the same melt as that from which the sample was taken and the ingot was sectioned to reveal the blow-hole structure.

The nitrogen, hydrogen and oxygen contents of samples taken from the

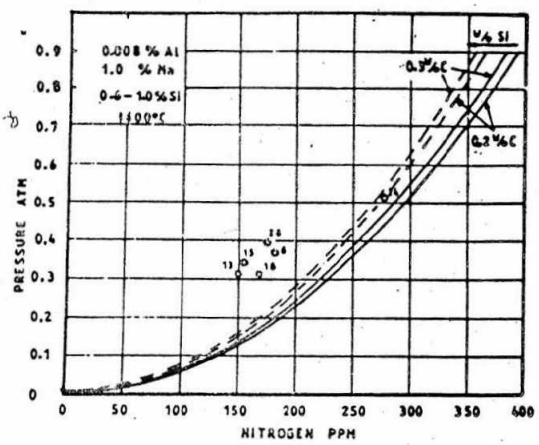

Fig.15 Experimental points obtained using the first bubble technique superimposed on a theoretical pressure versus nitrogen curve.

melts were analysed using conventional methods at some time after the ingots were cast.

5.2 Results and Technique Assessment

Since the melts used had high nitrogen contents, this element was used as a base for an assessment of the technique. For nitrogen contents determined subsequent to ingot casting the equivalent nitrogen gas pressures were calculated using Sievert's Law and the necessary parameters for the steel considered. Figure 15 shows the theoretical curves so derived for two different carbon contents. The pressures measured by the first bubble technique are shown as numbered circles and are some way above the curve in each case. Although carbon and silicon contents change the position of the curve, as shown, this does not account for the discrepancy. The hydrogen content of the melt was known to be on average 5 ppm, hence the contribution of hydrogen was determined using the method as in the one used for nitrogen. This gave a value of P_{H_2} of ~ 0.045 atm.

Assuming that the P_{N_2} value for a given nitrogen content and for a given alloy can be read from fig.15 and P_{H_2} can be added to this then the total pressure P_T^{fb} as given by the first bubble technique, $(P_{N_2} + P_{H_2})$ is equal to P_{CO}. For a given alloy composition the equivalent oxygen content can be calculated from,

$$K_{CO} = P_{CO}/h_c \cdot h_o$$

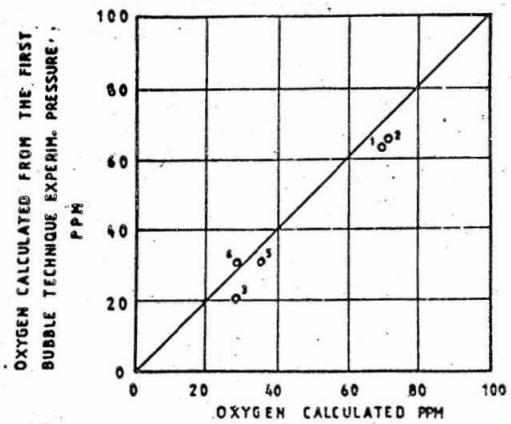

Fig.16 Oxygen deduced from the first bubble technique versus that calculated from deoxidation data.

where h_C and h_O are the Henrian activities of carbon and oxygen and K_{CO} is the equilibrium constant.

The theoretical oxygen content was calculated from relevant thermodynamic data assuming deoxidation by silicon, silicon-manganese or silicon-manganese-aluminium was controlling the oxygen content. Figure 16 shows that the "measured" oxygen content by the first bubble technique agrees well with the theoretically determined values.

5.3 Assessment of Blow-hole Behaviour Using the Technique

In a case where a large amount of aluminium was added and therefore the P_{CO} was very low, it was assumed that only nitrogen and hydrogen were contributing to P_T in the first bubble technique. In experiments where blow-holes were produced by increasing the nitrogen content a direct correlation was found between the onset of blow-hole formation and the value of P_T. That is, it was possible to predict whether or not the ingot was sound from the P_T value.

So far experiments have been carried out at only two carbon levels but in each case a critical P_T was found which when converted to a nitrogen content showed excellent agreement with the previous results.

5.4 Overall Assessment

The first bubble technique has been satisfactorily developed experimentally and it shows that the pressure measured relates to blow-hole formation in small ingots. In conjunction with an oxygen probe, not used here, to measure the active oxygen content, and therefore, P_{CO}, the contributions of nitrogen and hydrogen can be assessed as revealed by the calculations. It is intended to carry out further experiments along these lines to more fully evaluate the technique and its potential use as a tool in controlling ingot structure.

Fig.17 'Channels' revealed when an ingot was accidentally drained.

6. The formation of Macrosegregates

The origin and formation of crystal structure in ingots have been studied extensively and the parameters that influence such phenomenon as the extent of columnar growth are well-known. Probably of greater importance, however, are the factors that lead to the formation of macrosegregates, the typical A and V segregates in particular in ingots and to the non-uniform distribution of inclusions. Figure 17 shows interdendritic channels revealed by accidental liquid drainage from a large casting.

It is now widely accepted that macrosegregates generally, and channel segregates in particular, are primarily the result of interdendritic fluid flow during solidification. Increasing evidence has been produced over the last twelve years that the principle driving force for such fluid flow is gravity acting on thermosolutal density gradients in the mushy zone.

The importance of fluid flow in macrosegregation was demonstrated by Flemings and co-workers in a series of papers[6-9] aimed initially at a complete description of inverse segregation. A set of equations were derived which not only allowed the calculation of the final average composition of a small volume element (and hence the macrosegregation) but also gave the interdependence of fluid velocity, pressure, fraction liquid and liquid composition at any point in the mushy zone[6]. They also described how, when the effects of gravity were included in the equations[9], it would be possible for an unstable situation to occur when interdendritic liquid moved faster than and in the same direction as the isotherms. A similar treatment by Japanese workers[10] extended the work to consider the effects of small perturbations and came to the same conclusions: that under the influence of gravity the fluid flow pattern could be such that cold solute rich liquid flowed into hotter regions relatively depleted in solute. In an attempt to attain solutal equilibrium this liquid would melt the surrounding (solute depleted) dendrite arms, thus decreasing the resistance to further flow and ultimately produce a channel.

It is this mechanism which has, at various times, been proposed as the cause of the channel type segregates found in a wide variety of situations, e.g. freckles in ESR and VAR and in non-ferrous ingots, A-segregates in steels, streaks in cast rolls, etc. McDonald and Hunt,[11,12] for instance, conducted experiments which demonstrated that, in the NH_4Cl/H_2O analogue system at least, A-segregates were the result of convection in the mushy zone due to liquid density differences. The same analogue was used later by Asai and Muchi to test their perturbation calculations.

Copley et al[13] also used the NH_4Cl/H_2O system, this time to investigate freckle formation in VAR and ESR. They found that freckles were controlled not only by gravity, but also aligned with the heat flux. This thermal dependence was further demonstrated by the observation that when the growth rate and temperature gradient were increased the number of active channels decreased. They claimed that the situation was analogous to the oceanographic phenomenon termed the "perpetual salt fountain" important as a means of stirring the oceans.[14] Study and analysis[15,16] of the salt fountain have shown that the convective channels or filaments depend on a thermohaline Rayleigh number, and that as this number increases the channel size decreases and the fluid velocity increases.[15] The analysis also makes the points that a simple density inversion is neither required nor sufficient for motion and that the effects of both the thermal and the solutal contributions to the density gradient must be considered.

The similarity between channel type flow and the oceanographic case was also noted recently by Szekely and Jassal[17] in their theoretical analysis of the convective fluid velocities to be expected with both the bulk liquid and the musy zone of an NH_4Cl/H_2O casting. They were able to check their results using Schlieren photography and found quite good agreement between observation and prediction, with convection in the mushy zone occurring in the opposite direction to and at a velocity approximately 1/10th that of the bulk liquid convection.

More recently workers have tended to move away from the use of non-metallic analogues and many have preferred to use low melting point alloys such as tin-lead and aluminium-copper systems[18-21]. While some experiments on such systems have indicated that the bulk liquid has little influence on the mushy zone[22], it is clear that the opposite is not the case. Fredriksson and Nilsson's recent experiments[23] on tin-lead alloys appear to have confirmed earlier observations in the NH_4Cl/H_2O system[11] that the region of positive segregation in the top half of ingots is the result of rejected solute being carried from the mushy zone to the bulk liquid through A-segregates.

Possibly a more important aspect of the work done on metal systems is that of producing channel type segregates under controlled conditions.[19,21,24,25] Streat and Weinberg's work with lead-tin alloys[24] has shown that freckle-type channel segregates appear to originate from widening interdendritic channels in the interior of the ingot. Suzuki and Miyamoto[26] have developed a furnace capable of solidifying approximately 14kg of steel under controlled conditions. This was used to simulate the thermal characteristics of a much larger solidifying body in a conveniently sized sample. They too produced channel segregates and

were able to draw a relationship between the alignment of channels and the solidification rate. Lately they have begun to look at some of the factors controlling A-segregate formation and appear to have highlighted an important link with silicon content[27] an idea supported by Fujii et al.[28]

The most serious drawback to working solely with metal systems as above is that the process of solidification cannot be followed from start to finish. At best that process is interrupted part way through and a subsequent post-mortem investigation carried out. Some workers[22,29-31] have attempted to surmount the problem by the addition of radioactive isotopes, but with only limited success.

Thus a reasonably complete picture exists of how channel type segregates develop once fluid convection has started. Channels have been formed under controlled conditions in a variety of systems and some ways to eliminate them have been suggested.[32] In addition investigations have been made into the factors controlling both the fluid flow and the thermosolutal density gradients[28] in the mushy zone. Despite this we are still unable to explain the observation that sometimes in two nominally identical castings channel segregates occur in one but not in the other.[33]

The work presented here forms part of a larger programme of research aimed at explaining the above observation by looking more closely at some of the factors affecting both the initial formation of a channel and the thermosolutal density gradient which drives it. In this part of the work this is being attempted through continuous observation of solidification using an in-situ radiographic observation technique.[34]

6.1 Experimental Method

Equipment

The equipment was essentially that developed by Miller, Beech and Stephenson to allow direct observations to be made of the solidification of a small sample of metal. Fig.18 shows the arrangement of apparatus, a complete description of which is already available. The x-ray vidicon was connected to a video-tape recorder to allow real time recordings of the experiments. These were then replayed through an ordinary television monitor and still photographs taken every one or two minutes for subsequent analysis and study.

Alloy

The alloy chosen for study was Al-22.7 Cu. This had already been shown to meet the restraints of the melting unit and to provide adequate contrast through the vidicon system. The alloy has a liquidus of approximately 590°C, a partition coefficient $k \simeq 0.17$ and solidifies to a eutectic at 548°C and at 33.2wt.%Cu.

Sample preparation

The samples were sliced from a bar 19 mm x 11 mm cross section and polished in a jig down to $\simeq 300\mu m$ thick. Immediately before insertion into the apparatus the faces of the sample were lightly polished with fine grinding paper to minimise any effects of surface oxides.

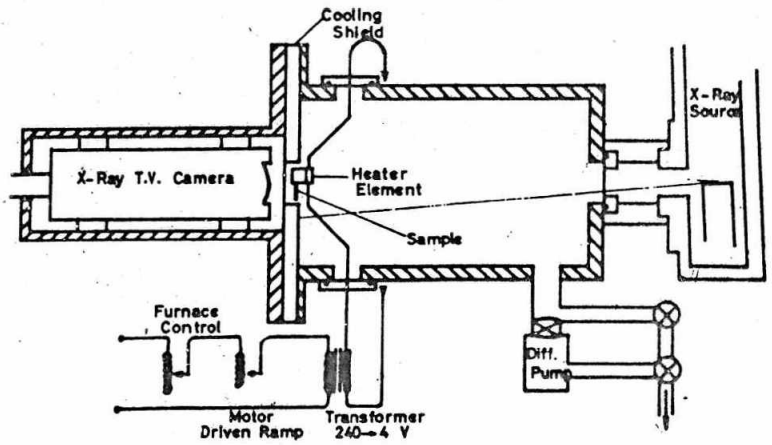

Fig.18 Schematic view of the apparatus.

Growth rate and temperature gradient measurement

In each sample the cooling rate ($\dot{T}$) was measured by a thermocouple on the graphite sample holder adjacent to the heater. The accuracy of the couple was checked by comparing the reading as the liquidus passed it with the known liquidus value of 590°C. The growth rate (R) was measured at mid screen height from a growth distance against time curve drawn from the series of still photographs. The temperature gradient (G) was measured in early experiments using thermocouples placed at intervals on the graphite sandwich. Subsequent values of G were estimated using the relationship:

$$RG = \dot{T} \qquad (7)$$

This was also used to check the self consistency of the results of the early experiments.

6.2 Results and Discussion

The table lists the cooling and growth rate data for the experiment reported here. The values of G vary from 2 to 5°C mm^{-1} which is a measure of the reproducibility of the temperature gradient in this experiment.

exp	$\dot{T}$ °C sec^{-1}	R $\mu m\ S^{-1}$	G °C mm^{-1}	θ	Tan θ
1	-	3.8	-	15	0.27
2	0.047	12.0	4.0	25	0.47
3	0.083	18.3	4.6	35	0.70
4	0.117	28.3	4.5	40	0.84
5	0.031	13.8	2.2	25	0.47
6	0.088	43.3	2.0	50	1.19
7a	-	25.0	-	40	0.84
7b	0.013	4.2	3.2	19	0.29
8a	0.118	33.0	3.6	45	1.00
8b	0.038	12.0	3.2	25	0.47
9	0.017	3.3	5.0	10	0.18

In this series of experiments the concern was with the formation of

Fig.19 Sequence of photographs showing the copper standards and the liquid and liquid + solid regions

(a) 2 mins after growth started, (b) 15 mins, (c) 31 mins.

The growth rate is 10 ms^{-1} and the temperature gradient about 10°C mm^{-1}.

channel type segregates as they appear in ingots. Accordingly all the samples were solidified sideways, as seen in figs.19-21. These photographs were selected to highlight features common to the whole series of experiments, most notably the curvature of the liquid-mushy zone interface and the existence of reasonably well developed channels, which were also apparent in the subsequent microstructures (fig.22).

Channel formation

Comparison of figs.20 and 23 demonstrates that channels can be identified through the vidicon as a darkening of the structure within the mushy zone, especially where the channels cross well defined dendrite primary arms.

The development of the two major channel segregates in fig.20 appear to support Streat and Weinberg's[24] suggestion that channel segregates develop

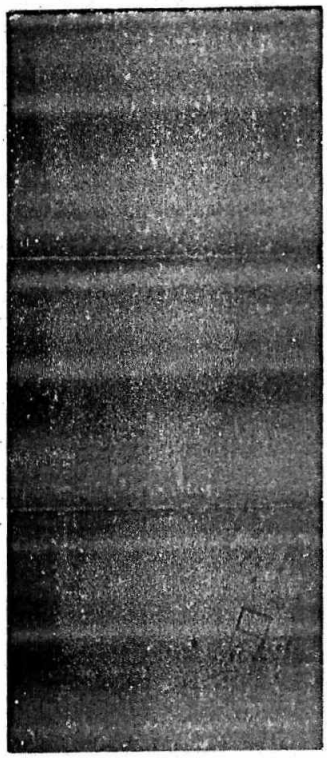

Fig.20 Sequence of photographs showing the development of two major channel segregates (A & B). The box in (c) is the area shown in Fig.22. The darker region on the left of the photographs was due to the extra thickness at the heater. (a) 4 mins, (b) 10 mins, (c) 19 mins after growth started. The growth rate is 5 ms^{-1} and the temperature gradient about 10°Cmm^{-1}.

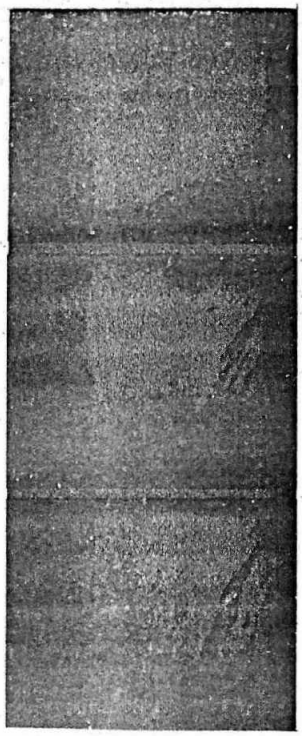

Fig.21 Sequence of photographs of channel development (a) 4 mins, (b) 15 mins, (c) 26 mins, after growth started. The growth rate is about 10 mm^{-1} and the temperature gradient 10°Cmm^{-1}.

from existing finer channels in the mushy zone. Unfortunately, since the edge of the sample was out of view, it was not possible to trace those channels back to their origin. In fig.21 however, and in other cases where the edge of the sample has been studied, it can clearly be seen that the major channel segregates originate at irregularities on the growth front resulting in the entrapment of a significant pocket of liquid by the advancing front. That such a situation could produce fluid flow is to be expected since the large driving force for fluid flow in this system would accentuate any instabilities caused by the irregular interface. It has already been shown[6-8] that macrosegregation can be significantly affected by relatively small changes in solidification conditions.

A large number of such irregularities would be expected during dendritic growth and the present observations have borne this out. That not all irregularities produce well developed channel segregates can be explained, in part at least, by two further observations. It will be noted in Fig.20(c) and 21(c) that the spacing between the channels is smaller closer to the liquidus. In addition some fine channels which were present early in solidification have effectively disappeared (figs.20(a)-(c)). These imply some mechanism for the 'annealing out' of the channels or for the rewelding of the dendrite mesh during solidification. A possible mechanism for such a process is suggested by the second observation, that the major channel segregates in fig.20 migrate towards the liquid-mushy zone interface during solidification.

It has long been recognised that one surface of an A-type segregate is normally sharp and well defined while the other is more diffuse and dendritic (fig.22). Although not very apparent

Fig.22 Micrograph of area marked in fig.20(a). Note the sharp boundary of the channels is on the side nearest the liquidus (the left).

at the small magnifications needed for reproduction here, the major channel (A) in fig.20 was observed to move up to about ½mm (i.e. approx. its own width) towards the liquidus during solidification. This observation is in agreement with the feeling of Fredriksson and Nilsson[23] that the smooth surface of a channel is the result of its melting action[9,11] and that the 'dendritic' front is exactly that; dendrites growing into a body (in this case a stream) of liquid. Thus, it can be envisaged that as a large channel develops it will draw liquid away from the surrounding regions. Any finer channels in these regions will suffer a consequent reduction in their remelting action along the sharp boundary, but will still continue to feed the dendrites along the other. Eventually they could heal up completely and be indistinguishable from the remainder of the dendrite mesh.

In considering the mechanism it should be remembered that the liquid in the channels will be of the eutectic composition only when it originates from and is till quite close to the eutectic interface. Away from that interface the liquid will either have

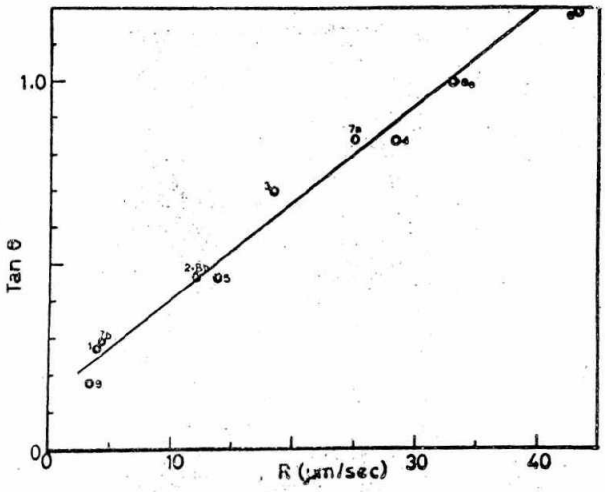

Fig.23 Plot of Tan θ versus growth rate (R) for the experiments in the table.

changed composition by remelting dendrite arms or have originated away from the interface and therefore be of a different composition anyway. The exception to this occurs during the final stages of ingot solidification when, as will be seen, even the bulk liquid can reach the eutectic composition.

The idea that only a few channels should grow and remain, moving about and adjusting shape during solidification, is a concept which is supported by the observations of Copley et al[13] on the disruption and subsequent re-formation of channels in the $NHCl/H_2O$ system, and the work of Stern[15] in relating channel size and numbers to the growth conditions.

Effect of growth rate on channel formation

The observations so far have been restricted to the formation and development of channels generally, as seen in the in-situ apparatus. The series of experiments was also concerned with the effects of horizontal growth rate. It was found that there was a clear variation in the alignment of the channels with growth rate. For each sample the angle θ, between the underside of the channel and the vertical, was measured and plotted against the measured growth rate R (fig.23). Where the growth rate changed during solidification the angle of the channel was plotted against the growth rate during the period in which the channel formed.

It was considered that, to a first approximation and ignoring other effects such as shrinkage, the velocity of the fluid in the channel would be the vector addition of a horizontal velocity (V_x) due to the growth rate (R) and a vertical component (V_y) due to gravity. Assuming that $V_x = R$, then (from vector addition)

$$\tan\theta = R/V_y \qquad (8)$$

The points in fig.23 should then form a straight line and it may be seen that they do.

Solute redistribution during solidification

The observation made using the in-situ technique are remarkably similar to observations made on large masses of steel and this is also true when solute redistribution is considered. The curvature of the liquid/solid interface is identical to that observed in earlier work. Solute-rich liquid has flowed to the bottom of the sample and so lowered the melting point and retarded growth at that point. This is analogous to the way in which solute concentrates in the central region of ingots.

Control of channel formation

The foregoing implies various solutions to the problem of channel formation. Some of these, such as increasing the freezing rate have some application in castings but are not so attractive in ingot prpduction. Recent work has shown that one solution lies in the control of the chemical composition which, if acceptable for other reasons, alters the composition of the interdendritic liquid in such a way that the decrease in density that occurs during freezing is minimised. However, the lack of data for distribution coefficients and the densities of dilute iron alloys prevents a detailed theoretical analysis. Work is at present in hand to obtain such data and hence approach more closely an analytical solution to the problem.

ACKNOWLEDGEMENT

The authors would like to express their appreciation to Martin Bridge, Ismael Saucedo and Juan Valencia who carried out the experimental work described in this paper.

REFERENCE

1. B.H.C.Waters, Metal Treatment and Drop Forging, 19 (1952) 379, 433, 474 and 527; 20 (1953) 79 and 103.
2. D.R.Thornton, J.Iron Steel Inst., 183 (1956) 300.
3. D.L.W.Collins, Metallurgia, 76 (1967), 10) 127.
4. R.J.Sarjant and M.R.Slack, J.Iron Steel Inst. 212 (1974) 428.
5. S.N.Tiwari and J.Beech, Metal Science, 12 (1970) 356.
6. G.E.Nereo and M.C.Flemings, Trans AIME 239 (1967), 1449.
7. M.C.Flemings et al, Trans AIME 242, (1968), 41.
8. M.C.Flemings and G.E.Nereo, Trans AIME 242, (1968) 50.
9. R.Mehrebian et al, Met. Trans 1, (1970) 1209.
10. S.Asai and I.Muchi, Trans. ISIJ 18, (1978), 90.
11. R.J.McDonald and J.D.Hunt, Trans. AIME 245 (1969) 1993.
12. R.J.McDonald and J.D.Hunt, Met. Trans, 1,(1970) 1787.
13. S.M.Copley et al, Met. Trans.1, (1970) 2193.
14. A.Stommel et al, Deep Sea Research 3,(1956) 152.
15. P.Stern, Tellus 12, (1960) 172.
16. J.S.Turner, Deep Sea Research 14, (1967) 599.
17. J.Szekely and A.S.Jassal, Met.Trans 9B, (1978) 389.
18. F.J.Hebditch and J.D.Hunt, Met. Trans 5,(1974), 1557.
19. N.Streat and F.Weinberg, Met.Trans 3,(1972) 3181.
20. D.Jaffrey, Met. Sci, 9,(1975) 13.
21. R.Mehrebian et al, Met.Trans 1, (1970) 3238.

22. M.J.Stewart and F.Weinberg, Met. Trans 3, (1972) 333.

23. H.Fredriksson and S.O.Nilsson, Met. Trans. 9B , (1978) 111.

24. N.Streat and F.Weinberg, Met.Trans. 5,(1974) 2539.

25. N.Streat and F.Weinberg, Met. Trans. 7B (1976) 417.

26. K.Suzuki and T.Miyamoto, Trans ISIJ 18, (1978), 81.

27. K.Suzuki et al, 6th Int, Vac. Met. Conf., San Diego, April, 1979.

28. T.Fujii, D.R.Poirier and M.C. Flemings, Met. Trans. 10B, (1979).

29. K.Andrews and C.R.Gomer "Solidification" p.363 (1968) Iron and Steel Institute P.110.

30. F.Weinberg et al "Solidification and Casting" p.334 (1979), Metals Society Book 192.

31. D.J. Hebditch and J.D.Hunt, Met. Trans, 4, (1973) 2008.

32. M.C.Flemings, J.Scand.Met. 5, (1976) 1.

33. R.Hickley and W.A.Turner, Davy Roll Co. Ltd., - private communication.

34. M.P. Stephenson and J. Beech, "Solidification and Casting" p.34, (1979) Metals Society, Book 192.